Adhesion Force Between Fine Particles with Controlled Surface Properties

M. A. S. Quintanilla, J. M. Valverde, and A. Castellanos
Faculty of Physics, University of Seville, Avenida Reina Mercedes s/n, 41012 Seville, Spain

DOI 10.1002/aic.10770
Published online February 13, 2006 in Wiley InterScience (www.interscience.wiley.com).

The adhesion force between previously consolidated polymer particles is affected by the use of additives that modify relevant surface parameters, such as the contact hardness and size of asperities at contact. Both the size of silica nanoparticles uniformly coating the particle surfaces, and their surface coverage have been investigated. The effects of the presence of other additives, such as wax and cross-linking polymer were tested. The experimental results are compared with predictions from theoretical models. Our measurements are shown to be in semi-quantitative agreement with the theoretical expectations built on the hypothesis of plastic flow of interparticle contacts. Moreover, the results indicate that the aggregation of individual particles in the fluidlike regime must play a relevant role in how bulk stresses distribute among interparticle contacts when the powder transits to the solid state. This work highlights the need of considering particle aggregation and contact plasticity as central features, mostly obviated so far, to deal with real problems on cohesive powders. © 2006 American Institute of Chemical Engineers *AIChE J,* 52: 1715–1728, 2006

Keywords: fine powders, cohesion, fluidization, agglomeration, van der Waals force, powder compaction, contact plasticity

Introduction

The flow behavior of fine powders is recognized nowadays as a keystone of many high-tech industrial processes. Ultimately powder flowability depends on interparticle interaction, which is governed by parameters such as particle size, shape, roughness, hardness, and so on. Yet interparticle contact forces are difficult to control, model, and measure. Traditionally the ability of powders to flow has been roughly estimated from the size of their primary particles. With increasing fineness, the interparticle attractive force increases in comparison to the force of gravity, leading to the formation of stable arches that inhibit powder flow. A useful number to estimate flowability has been the granular Bond number (Bo_g), defined as the ratio of the interparticle attractive force to particle weight. As a rule of thumb, $Bo_g \gg 1$ implies strong cohesiveness and aggregative behavior (fine powders, for example), whereas if Bo_g is of order one, or smaller, cohesiveness is negligible and particles display an individual free-flowing behavior (dry granular materials). Numerical simulations[1] and experiments[2,3,4] show a fundamental role of Bo_g on the flow of fine particles. Yang et al.[1] have quantified by numerical simulations the effect of the size of hard spheres on the packing. They approximated the interparticle contact force to the van der Waals force F_{vdW} and found that the main parameter governing the packing was the ratio $F_{vdW}/W_p = Bo_g$, where W_p is the particle weight. Forsyth et al.[3] showed experimentally that the void fraction of a bed of magnetic spheres is linearly related to F_{ip}/W_p, where F_{ip} is the interparticle magnetic force. Although they speculated on the applicability of the same law to dry nonmagnetic fine particles, their predictions clearly underestimated the experimental packing fractions taken from the literature on fine powders. A major problem is that packed fine particles are generally consolidated by compressive forces (at least under the weight of the particles above), and the application of an external consolidating stress may increase dramatically the interparticle adhesion force.[5]

Correspondence concerning this article should be addressed to J. M. Valverde at jmillan@us.es.

Even attractive forces alone may cause an appreciable deformation of the contact surfaces having a profound effect on interparticle adhesion.[6] To take into account the increase of adhesion due to compressive loading some models built on the mechanics of frictional-cohesive spheres hypothesize that the parameter governing the behavior of a cohesive powder should be the ratio of the adhesion force to the compressive force per contact.[7] Nevertheless, it is uncertain that the ratio of these two forces should be a constant. A reliable estimation of contact forces is, therefore, a fundamental step to understand powder flow. A second open problem to understand the behavior of bulk cohesive powders is the structural organization of cohesive particles in aggregates. Particle aggregates exist in the fluidlike regime as a consequence of the strong interparticle attractive forces. The jamming of these aggregates in the fluid-to-solid transition determines powder compaction[8,9] and, therefore, aggregates should be considered in the transmission of external stresses within the bulk powder. In a recent work, Olson et al.[11] also show this relevant effect in avalanches of aggregates artificially made with glued beads.

In this article, we present measurements of the interparticle adhesion force as a function of the interparticle compressive force for fine polymer particles (particle size $d_p \sim 10$ μm) coated with surface additives. These experiments show quantitatively how the control of surface properties and particle aggregation may affect contact forces, and as a consequence powder flowability. The rest of this introductory section is devoted to a brief review on the basic theories of interparticle contact forces (a detailed review is given in [10]).

Theory on contact forces: Interparticle attractive force between rigid particles

Attractive forces between dry and uncharged fine particles are mainly attributed to van der Waals forces produced by the interaction of fluctuating molecular dipole fields.[12] Assuming that retardation effects are negligible and that the interaction between molecules is pairwise, Hamaker[13] summed up all the interactions between two spherical and rigid particles at contact with dia. d_1 and d_2, arriving at the approximate expression for the attractive force

$$F_{vdW} \simeq \frac{Ad^*}{12z_0^2} \tag{1}$$

where A is the Hamaker constant, $d^* = d_1 d_2/(d_1 + d_2)$ is the reduced diameter, and $z_0 \simeq 4$ Å[14] is the distance of closest approach between two molecules. Because of the short range of the molecular interaction, the van der Waals force is actually determined by the local radius of curvature of the surface asperities at contact. Therefore, the typical size of the surface asperities d_{as} must be used in Eq. 1 instead of the particle diameters.[15] A relevant consequence of the short range of interaction is, therefore, that interparticle attraction depends strongly on surface properties that can be altered by the use of surface additives. The control of interparticle forces by tailored surface additives has been experimentally demonstrated by measurements of the adhesion force using atomic force microscopy.[16] It is important to remark, however, that Eq. 1 is only strictly applicable to the case of not deformed contacts.

Theory on contact forces: Interparticle adhesion force between deformed particles

A relevant parameter in contact mechanics is the work of adhesion w, defined as the work needed to separate two half-spaces of an infinite body in an isothermal and reversible process in vacuum. Ideally, the work of adhesion must be equal to the energy stored in these two surfaces, that is $w = 2\gamma$, where γ is the surface energy of the solid. Experimental measurements of the work needed to separate two surfaces have given the correct order of magnitude of the surface energy of some ordinary solids and liquids. However, in many situations the force needed to separate two solid surfaces depends on the deformation mode, surface roughness and on the degree of contamination of the surfaces. If contamination by impurities or water vapor from air is relevant it may happen that the work of adhesion is much smaller than 2γ.[26] On the other hand, plastic deformation in the contact zone can lead to the opposite result.[26] Studies of wetting of nonplanar substrates have shown that roughness enhances the critical surface energy,[23] but on the other side, it is found that roughness reduces the adhesion force between elastic solids. It is clear, therefore, that the surface energy alone cannot account for the adhesion of contacting solids since the real area of contact due to surface roughness and bulk deformation have a great influence.

The pull off force (hereafter adhesion force F_t), is defined as the maximum tensile force needed to separate two particles. Under the action of attractive forces the particles deform elastically, and they may flow plastically in short contact times or viscoelastically/viscoplastically in longer times. As a result the adhesion force can be a function of the previously applied compressive (pull on) force (hereafter, compressive force F_c), and a set of physical parameters of the particle such as the Young's modulus, coefficient of Poisson, surface hardness, interfacial energy, radius of the particle, and local curvature at the area of contact. For longer times the adhesion force can be also a function of viscosity, or softening/hardening rules.

The determination of F_t as a function of the compressive and attractive forces acting between two particles comprises two steps. First, it must be known how the particles deform under the compressive forces until they reach the final equilibrium position, and second, the subsequent evolution of their profiles must be solved as the pull off force is applied in order to overcome attractive forces. The first problem (so called indentation problem) is quite complex as the particles begin to deform even before they touch each other due to the attractive forces among their molecules. Once the contact is established the particles continue to deform under the combined action of the external compressive force and the molecular attractive forces, the latter increasing during the indentation process as more and more molecules accumulate in the neighborhood of the contact area. This process is curtailed by the repulsive elastic stresses that develop in the bodies. However, if the attractive forces (alone or combined with the external compressive force) are high enough, parts of the body may overcome the elastic limit and a plastic flow will develop on short time scales and a viscoplastic/viscoelastic flow on larger time scales. The second problem of unloading is also of great complexity, as the profile of each particle under the presence of partial plastic flow, relaxation of elastic stresses and decreasing attractive forces must be calculated. This problem has defied

until now complete solution, and only in some limiting situations there exist analytical solutions. Though it is obvious that for purely elastic deformations, and, therefore, perfectly reversible, F_t will depend only on the attractive forces, and not on F_c, even the solution for this problem is not known in general. The aim of this section is just to give a brief review of the relevant theories for our work. The reader may find a detailed discussion in [10].

The Elastic Regime. The problem of finding the interparticle adhesion force has been solved for elastic deformations. Two apparently contradictory models were first proposed by Johnson, Kendall and Roberts (JKR)[18] and Derjaguin, Muller and Toporov (DMT)[19] for the adhesion force. Both approaches were later found to be valid for different limits of the Tabor parameter[20]

$$\mu = \left(\frac{d_{as}^* w^2}{2E^{*2} z_0^3} \right)^{1/3} \tag{2}$$

where $1/E^* = 2(1 - \nu^2)/E$, being ν the Poisson ratio, and E the Young modulus.

The theory yields an adhesion force

$$F_t = \chi \pi w d_{as}^* \tag{3}$$

where d_{as}^* is the reduced diameter of the asperities at contact, and χ may take values ranging from 3/4 ($\mu \gg 1$, JKR limit) to 1 ($\mu \ll 1$, DMT limit).

The JKR model assumes that the attractive forces are confined to the inside of the contact area, and a tensile pressure distribution is postulated along the circular contact surface ($p(r) = -p(0)(a^2 - r^2)^{-1/2}$, where r is the radial coordinate, and a is the contact radius). On the other hand in the DMT model, attractive forces are supposed to act outside of the contact area, and it is assumed that the deformed profiles of the bodies are given by the Hertz theory, which gives the deformation of the loaded contact between two nonadhesive particles. Then the maximum of the pull off force (adhesion force) occurs when the contact area reduces to a point.

Some approximate models have been published to describe the behavior of an adhesive elastic contact in the range of the Tabor parameter $0.1 < \mu < 5$.[21,22] In all these theoretical works the force of adhesion F_t is a function of μ only, and varies smoothly between the limits given by the DMT model and the JKR model. In any case F_t does not depend on the previously applied compressive force for purely elastic (reversible) deformations of the particle surfaces.

The Plastic Regime. Taking into account the Hertz solution for elastic solids the critical load on the contact for the initiation of plastic yield within the bulk has been found to be[24]

$$P_Y \simeq \frac{2\pi^3 (d_{as}^*)^2 Y^3}{3E^2} \tag{4}$$

where Y is a characteristic constant of the material known as yield strength in compression. Attractive forces contribute as an effective load P_0 on the contact, even in the absence of external compressive force, may originate by their own plastic deformation if $P_0 > P_Y$.[6] For zero external compressive force and negligible deformation the term due to attractive forces alone is $P_0 \simeq \pi w d_{as}^*$,[19] where $w = 2\gamma$. Thus, we estimate that attractive forces would induce plastic deformation ($P_0 >\sim P_Y$) if $d_{as}^* <\sim 3wE^2/(2\pi^2 Y^3)$. As the pressure is increased by external compression the plastic zone grows inside the bulk of the particle until it eventually reaches the contact surface and propagates along it.

In the regime where the whole area of contact deforms plastically (fully plastic regime), and provided that the deformation of the asperity is much smaller than the asperity size, the pressure on the contact area does not depend on the external compressive force, and is given by $p_m = H \simeq 3Y$ (H is the contact hardness).[25] Thus, the total load on the contact is obtained as $F_c = \pi a^2 H + F_{at}$, where F_{at} is the attractive force between the deformed spheres. Given the attractive force as a function of the contact radius a, this equation yields the final radius of equilibrium of the contact (a_f) when it is subjected to an external compressive force F_c. In order to find out F_t for a given F_c, Mesarovic and Johnson have recently considered that the material deforms elastically when the force is decreased during the pull off process (fully plastic deformation with elastic recovery).[26] Thus, the pressure upon unloading was taken as the solution for the elastic recovery of a circular area subjected to a constant pressure. The estimated adhesion force was

$$F_t \simeq \frac{3\sqrt{\pi}}{2} \frac{wE^*}{H^{3/2}} \sqrt{F_c} \tag{5}$$

It is important to remark that the pressure on the contact area retains its constant value p_m as long as the deformation of the asperity is small compared to its radius. This is generally expressed by the condition of small-scale-yielding that requires the plastic zone to be much smaller than the contact radius.[26] If the deformation of the asperity is not small, the plastic flow of the material from the central region to the surroundings of the contact area must be taken into account. The effect of this plastic flow is to pile up material at the edge of the contact area. The consequent increase of the contact area (over the value it would have if plastic flow were negligible) makes the value of p_m to decrease below $p_m = 3Y$ as the compressive force on the contact is increased.[26,28]

Back in 1976 Johnson[29] had arrived at a similar result by assuming that the net effect of the fully plastic deformation upon loading was to increase the local radius of curvature of the recovered profiles of the asperities at contact. Then he used the JKR solution for the pull off force and obtained

$$F_t \simeq \frac{2}{\pi} \frac{wE^*}{H^{3/2}} \sqrt{F_c} \tag{6}$$

More recently the Maugis model[21] has been used to compute the pull off force when attractive forces act also outside the contact. The ratio of the pull off force derived in that case to the pull off force given by Eq. 5 is in the range between 0.84 and 1.14. Therefore, it is reasonable to use the approximate Eq. 5 to estimate the pull off force as a function of the compressive force. However, Eq. 5 is applicable whenever the external compressive force is much larger than the load due to the

attractive forces since it has been obtained by neglecting the contribution of molecular attractive forces to the indentation process. To overcome this limitation, Maugis and Pollock[25] suggested in 1984 to substitute F_c by $F_c + \pi w d_{as}^*$ in Eq. 6 (further discussion on this topic can be found in [10]). If we apply the same argument to the more recent Mesarovic-Johnson improved approach (Eq. 5), we arrive at the modified Maugis-Pollock equation

$$F_t \simeq \frac{3\sqrt{\pi}}{2} \frac{wE^*}{H^{3/2}} \sqrt{F_c + \pi w d_{as}^*} \tag{7}$$

The indentation and decohesion processes may be far more complicated. We may have for example partial flow with partial elastic recovery, and in this case we would be in between the ductile and brittle breaking regimes (corresponding to purely elastic unloading). Mesarovic et al.[26] and Maugis and Pollock[25] propose an adhesion map in order to consider these various possibilities. A more complicated situation is the elastoplastic loading regime that occurs when the region of plastic deformation upon loading is smaller than the contact area[30] as can be the case in the region of very small compressive forces.[31] A detailed discussion on this case is given in [10]. In the interpretation of our experimental results we will not consider it since the scatter of the experimental data is larger than the small deviation theoretically expected from the analytical result given by Eq. 7.[31]

Experimental Powders

The powders used for the experimental study are xerographic toners based on polymer (particle density $\rho_p \simeq 1.1$ g/cm^3). Toner particles are produced by an attrition process, thus, having an irregular shape. Attrition is followed by size classification using a cyclone separator apparatus. Aerodynamic classification produces a narrow particle-size distribution. Powders of volume average particle diameter between dp $= 7$ μm and 19.1 μm have been obtained in this way for testing. In the preparation of some of the powders a cross-linking agent (gel) has been added to the parent polymer in different amounts. This causes a slight increase of the contact hardness (from $H \simeq 0.42$ GPa at 30% gel to $H \simeq 0.45$ GPa at 45% gel).[32] We have also tested special toners formulated with wax.

For polymer-polymer contacts ($w \simeq 0.07$ J/m^2, $\nu \simeq 1/3$, $E \simeq 6$ GPa[5]) we get a value of the Tabor parameter $\mu \sim 1$, which is between the JKR and DMT limits for the adhesive force between elastic contacts. However, in the case of our polymer particles ($Y \simeq 0.1$ GPa[5]), Eq. 4 gives $d_{as} <\sim 0.8$ μm for the critical asperity size below which plastic deformation is present. This value is clearly larger than the typical asperity size estimated for most powder particles.[33] Thus, the elastic limit is well exceeded due to the presence of attractive forces alone, and according to the modified Maugis-Pollock equation (Eq. 7) we should expect a nonlinear dependence of the adhesion force with the compressive force. Since, the compressive forces applied in our measurements are small we will admit the validity of the assumption that the plastic zone at the maximum compressive force is much smaller than the contact radius for Eq. 7 to be applicable. Moreover, the interparticle adhesion force measured is reproducible after many loading-unloading cycles, indicating that the asperity size has not been essentially affected during compression in the range of small compressive forces applied.

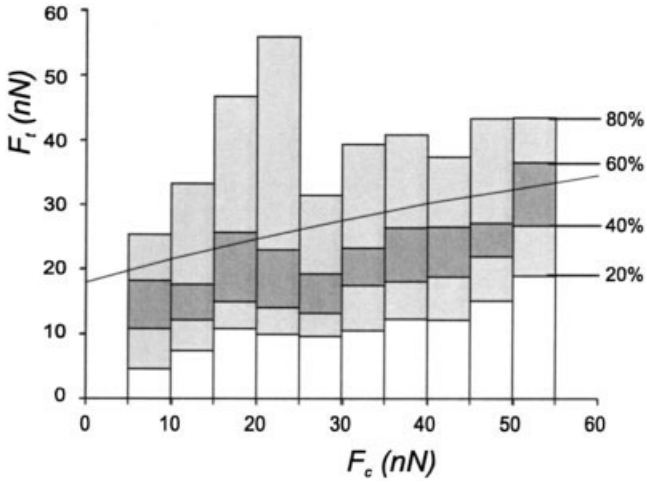

Figure 1. Statistics of the cumulative distributions of the adhesive force measured using an atomic force microscope between two xerographic toner particles with low additive coverage (10% *SAC*), as a function of the previously applied compressive force.

The continuous line is the predicted force by the modified Maugis-Pollock equation (Eq. 7) with: $E = 6$ GPa, $\nu = 1/3$, $H = 300$ MPa, $w = 0.07$ J/m^2, $d_{as} = 0.2$ μm.

The adhesion force between individual toner particles has been measured as a function of the compressive force using an atomic force microscope as reported elsewhere.[5] In this instrument a probe particle is attached at the end of a "V" shaped tipless cantilever. The probe particle is brought close to an isolated substrate particle under computer control, and a loading-unloading cycle is applied. The largest downward deflection achieved by the cantilever during unloading gives the adhesion force. Figure 1 shows the statistics of the cumulative distribution for F_t measured on different ranges of the compressive force. The continuous line is the theoretical prediction according to Eq. 7.

The toners are blended with a flow control additive consisting of fumed silica nanoparticles. Silica nanoparticles used here have two different nominal diameters, $d_s = 8$ nm, and $d_s = 40$ nm. (Both are fumed silica treated with hexamethyldisilazane, rendering the silica extremely hydrophobic.) Additive concentrations tested range from 5% to 100% of theoretical surface area coverage (*SAC*). The value of *SAC* is calculated assuming that the silica nanoparticles are individually distributed on the toner particle surface. A detailed analysis of SEM micrographs carried out by Ott and Mizes[16] on similar xerographic toners revealed however that the 8 nm silica nanoparticles are distributed in agglomerates with estimated diameters $d_{ag} \sim 50$ nm. Likewise, we see that the 40 nm silica nanoparticles are aggregated in agglomerates of estimated diameters $d_{ag} \sim 200$ nm (Figure 2). From our SEM micrographs and from higher quality micrographs obtained by Ott and Mizes,[16] we can conclude that the coating of these agglomerates on the toner particle surface is random and uni-

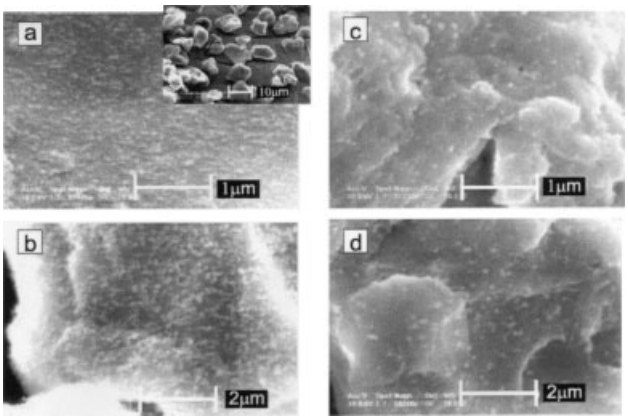

Figure 2. SEM micrographs of the surface of toner particles coated with silica nanoparticles of different sizes (a) 8 nm and 100% *SAC* (b) 40 nm and 100% *SAC* (c) 8 nm and 20% *SAC* and (d) 40 nm and 20% *SAC*.

The inset of Fig. a) shows a general view of toner particles.

form (see for example Figure 2). For most powder particles the local radius of curvature of surface asperities is often not larger than 0.1 μm,[15,33] thus, a good approximation for our bare polymer particles could be $d_{as} \simeq 0.2$ μm. This typical size can be decreased down to the size of silica agglomerates if a high surface additive coverage is used.

The theoretical surface area coverage of additive *SAC* is related to the weight percentage of additive (%wt), which is the controlled parameter, by the equation

$$SAC = N_{ag} N_s \frac{d_s^2}{4d_p^2} = \frac{\rho_p}{\rho_s} \frac{d_p}{4d_s} \,(\%\text{wt}) \tag{8}$$

where N_{ag} is the number of agglomerates on the toner surface, $N_s = f d_{ag}^3 / d_s^3$ is the number of silica nanoparticles per agglomerate (f is the solid volume fraction of the agglomerate), and ρ_s is the silica density ($\rho_s \simeq 2.2$ g/cm^3). On average, the number of silica agglomerates N_{ag} on the toner surface can be estimated as

$$N_{ag} \simeq \frac{\pi d_p^2}{A_{ag}} \tag{9}$$

where A_{ag} is the effective area of the toner surface corresponding to an agglomerate. Due to agglomeration of silica nanoparticles, their real surface coverage on the toner particle is given by

$$SAC^* = \frac{d_s}{d_{ag}} \frac{1}{f} SAC < SAC \tag{10}$$

Silica agglomerates are formed through a previous milling process where transient consolidation pressures may be high. Thus, even though individual silica nanoparticles are highly cohesive, f can be close to the random packing limit of noncohesive spheres (we will use $f \sim 0.5$).

In order to evaluate the effect of the additive on interparticle contacts it is important to estimate the *SAC* values at which there is a crossover in the nature of contacts from polymer-polymer to polymer-silica (SAC_{ps}), and from polymer-silica to silica-silica (SAC_{ss}) as the additive weight percentage is increased.

Figure 3a shows an idealized picture of the contact between two coated toner particles in two critical situations. In (a) we have the situation at which the polymer-polymer contact would change to polymer-silica contact for slightly higher additive concentrations. In (b) we have the situation at which the polymer-silica contact would transit to silica-silica contact for slightly higher additive concentrations. It can be derived from Figure 3a that for separation distances between silica agglomerates of the same toner particle smaller than $2d_{ia} \simeq 2\sqrt{2d_l d_{ag} + d_{ag}^2}$, polymer-silica contacts start to be more likely that polymer-polymer contacts. Thus, $A_{ag} \simeq 4d_{ia}^2 \simeq 8d_l d_{ag} + 4d_{ag}^2$, and from Eqs. 8 and 9 we estimate

$$SAC_{ps} \simeq f \frac{\pi}{16} \frac{d_{ag}^2}{(2d_l + d_{ag})d_s} \tag{11}$$

Here d_l is the diameter of the surface local curvature, which for the 50 nm silica agglomerates (8 nm silica particles) can be taken as the typical surface asperity size $d_l \simeq d_{as} \simeq 0.2$ μm. On the other hand, 40 nm silica particles form agglomerates of

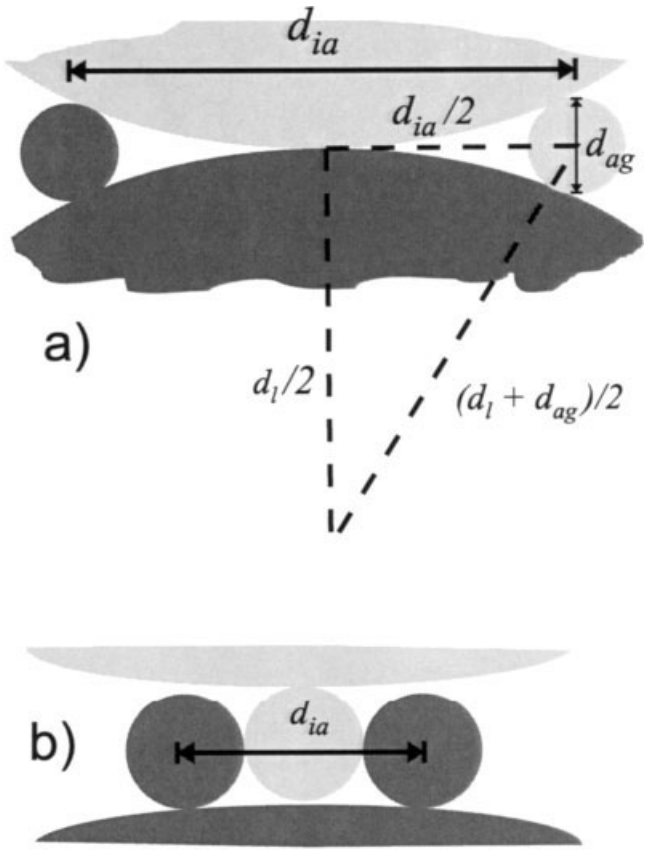

Figure 3. Illustrations to estimate the surface coverage of silica at the transitions in the nature of contacts from polymer-polymer to polymer-silica, (a) and from polymer-silica to silica-silica (b).

the order of this size and, therefore, cannot see surface asperities at this level. For such large additive agglomerates, we take for d_l the diameter of surface local curvature at a micrometric scale, which from SEM micrographs is $d_l \sim 1$ μm typically. The calculations yield $SAC_{ps} \simeq 7\%$ for the 8 nm additive particles and $SAC_{ps} \simeq 4\%$ for the 40 nm additive particles.

Figure 3b illustrates the situation at which the surface coverage of additive is sufficient to produce a majority of contacts between silica agglomerates. In that case the separation distance between silica agglomerates of the same particle is $2d_{ag}$ and, thus, $A_{ag} \simeq 4d_{ag}^2$. From Eqs. 8 and 9, we estimate

$$SAC_{ss} \simeq f \frac{\pi}{16} \frac{d_{ag}}{d_s} \tag{12}$$

which gives $SAC_{ss} \simeq 61\%$ for the 8 nm additive particles, and $SAC_{ss} \simeq 50\%$ for the 40 nm additive particles ($SAC^* \simeq 20\%$). It must be expected, therefore, that flow properties experience a marked change when SAC is varied within the range between SAC_{ps} and SAC_{ss} as seen, for example, in the dependence of the packing and tensile yield stress on the consolidation stress.[8,34]

Estimation of Contact Forces from Bulk Stresses

Measurement of bulk stresses

The sevilla powder tester (SPT) is a fluidized bed apparatus designed to measure the average particle volume fraction (ϕ), and tensile yield stress (σ_t) of fine cohesive powders as a function of the bulk consolidation stress applied previously (σ_c). The SPT functioning has been reported elsewhere in detail,[35] and we give here only a brief summary. The powder sample is held in a vertically oriented cylindrical vessel (4.42 cm internal diameter), and rests on a sintered metal porous filter (5 μm pore size), which serves as a gas distributor. By means of a series of computer controlled valves, and a mass flow controller a controlled flow of dry nitrogen is pumped upward or downward through the bed, while the gas pressure drop across it is read from the differential pressure transducer. All the measurements are preceded by a convenient initialization of the sample into a reproducible state. This is accomplished by imposing a high upward gas flow that drives the powder into a bubbling regime in which it looses memory of its previous history.[36] The gas flow is then turned off, and the particles settle into a standardized packing state as a preliminary to testing. The consolidation stress in this initial state at the bottom of the sample is given by its own weight per unit area W, which typically is $W \sim 100$ Pa. Wall effects are negligible for shallow beds, with heights typically smaller than their diameter.[34] The SPT provides us with a useful technique to test the powder under very low-confining pressures like in microgravity. To decrease σ_c below the powder weight per unit area, we allow the powder to settle under a small upwards directed gas flow. In this way σ_c is lowered down to

$$\sigma_c = W - \Delta p_0 \tag{13}$$

where Δp_0 is the pressure drop of the remaining gas flow. In this way the powder can be tested under consolidation stresses as low as a few Pascals.[8]

On the other side, in order to compress the powder over its own weight, the path of the gas can be inverted and the, now downward directed, gas flow is increased slowly. This imposes a homogeneously distributed pressure on the powder, pressing it against the distributor plate. The consolidation stress at the bottom of the bed is, thus, increased, and is given by Eq. 13, where now $\Delta p_0 < 0$. Further increases of the compressing gas flow imposes larger pressures on the sample.

The height of the bed h, which gives an average value of the particle volume fraction ($\phi = m_s/(\rho_p A h)$) is measured by an ultrasonic sensor placed on top of the vessel. This device determines distances with an accuracy of ± 0.01 cm (much smaller than local fluctuations in bed height), by sending an ultrasonic wave and measuring the time of reflection from the target.

In order to measure the tensile yield stress the gas flow is slowly increased in the upward direction to put the bed under tension. When the gas passes through the packed bed of particles, the gas pressure drop arises from the frictional resistance and increases linearly with increasing gas flow at low Reynolds numbers as described in general by the Carman-Kozeny equation.[37] At the minimum fluidization gas velocity the gas pressure drop Δp_m balances the weight of the powder per unit area ($\Delta p_m = W$), but cohesive forces prevent it from failure even if the gas velocity is further increased. The powder breaks at the bottom, and Δp falls abruptly when the gas velocity reaches a point at which the excess in pressure drop equals the powder tensile strength. The overshoot of Δp over W gives us then a quantitative measure of the tensile yield stress σ_t of the previously consolidated sample.[34]

Estimation of contact forces

The average interparticle compressive force F_c, and adhesion force F_t, can be estimated from measurements of the bulk stresses (consolidation stress σ_c, and tensile yield stress σ_t, respectively), and average particle volume fraction ϕ using the Rumpf averaging equation[38]

$$\sigma_i \sim F_i \frac{\zeta \phi}{\pi d_p^2} \tag{14}$$

where the subscript i stands for either consolidation or adhesion depending on the averaged force. Here, ζ is the coordination number (average number of contacts per particle). Equation 14 was originally derived by Rumpf for an ideal packing of hard spheres, wherein the distribution of stresses is isotropic and homogeneous, however, our experimental setup corresponds to closed-die compaction. From the theorem of virtual works, Emeriault and Chang[39] studied the effect of an anisotropic distribution of contacts. Their analysis showed that the stress tensor σ_{ij}, and the interparticle contact force F_i could be related by the equation

$$F_i = \sigma_{ij} n_k A_{kj} \tag{15}$$

where n_i is the unit vector along the contact orientation, and A_{ij} is the inverse tensor of the fabric tensor, which is defined as[39]

$$F_{ij} = \frac{d_p}{V} \sum_c n_i^c n_j^c \tag{16}$$

In Eq. 16, the summation extends over all contacts in the volume V, and n_i^c represents each unit vector perpendicular to the surface of the particle at the contact point. Emeriault and Chang assumed that all contacts in the same orientation carry the same contact force. This hypothesis allowed them to calculate the fabric tensor for a given contact angular distribution and coordination number.[39] Then Eq. 15 can be used to derive contact forces from stresses. In the particular case of an isotropic contact angular distribution and a uniaxial stress tensor, Eq. 14 was recovered.[39] In ref. [5] we have analyzed the effect of an anisotropic contact angular distribution resulting from a uniaxial compression of the powder, and we arrived at the equation

$$F = \frac{\pi d_p^2}{\phi k} \sigma \left(1 + \frac{2}{\sqrt{5}} \zeta \right)^{-1} \tag{17}$$

which differs from Eq. 14 only by a multiplicative factor. For a 2-D system $\zeta \sim 0.1$,[40] representing a decrease of only a 10% in the contact force. Even though we are dealing with a 3-D system, it can be expected that the deviation from the Rumpf equation should not be significant. Storakers et al.[41] have developed a micromechanical model for powder compaction under the assumption of affine deformation,[41] which is able to relate the compaction pressure to the particle volume fraction (so called relative density). The behavior of powder compacts under either isostatic or close die conditions has been also modeled by DEM simulations[42] that show reasonable agreement with experimental results on the effective Young's modulus. In these work, the initial relative density is around the random close packing fraction ($\phi_{RCP} = 0.64$), and extends up to values close to 0.95, which are achieved in the cold compaction of metallic powders and require the application of pressures of a few hundreds of MPa.[43] We must remark that this range is far beyond the range of volume fraction of our experiments performed at very low-consolidation pressures (typically we have $\phi < 0.4$ for $\sigma_c < 10$ kPa). It is worth noting, however, that although the effective Young's modulus of the compact under isostatic conditions is significantly lower than for close die conditions, the results tend to converge at the limit of $\phi \simeq \phi_{RCP}$.[42] Likewise, although the model by Storakers et al.[41] yields a significant difference between the axial stress and the transverse stress in close die compaction, both stresses converge in the limit of random close packing. From these studies, it is reasonable to expect that the distinction between isostatic and close die conditions will not be relevant in our study.

In [5] we analyzed also the effect of polydispersity and we arrived at the conclusion that it does not represent an important correction either.[5] In this work we will investigate the effect of particle aggregation in cohesive powders on the distribution of contact forces.

The relation between ζ and ϕ in systems of randomly packed particles has been a subject of research for many years (see [44] for a review), and it is common knowledge that the mean coordination number increases with increasing particle volume fraction. In their review Suzuki et al.[44] concluded that the simple equation

$$\zeta \simeq \frac{\pi}{2} (1 - \phi)^{-3/2} \tag{18}$$

(valid for $\phi > 0.18$), derived by Nakagaki and Sunada[45] from computer simulation using a random-packing model, was a satisfactory representation of most empirical and computational results. More recent investigations uphold this conclusion: Equation 18 has been successfully employed by Jaraiz et al.[46] to give a prediction of the Geldart C/A transition. The trend shown by Eq. 18 has been derived from a computer simulation of the compaction process of an assembly of cohesive particles, where the effect of cohesion in preventing contact restructuring was simulated introducing a critical contact angle.[47] Yang et al.[1] have recently presented a simulation of the packing of fine cohesive particles, based on the distinct element method (DEM), where the dominant van der Waals attractive force is explicitly considered. Their results on the coordination number for $\phi <\simeq 0.6$ are summarized by the equation

$$\zeta = 2.02 \frac{1 + 87.38\phi^4}{1 + 25.81\phi^4} \tag{19}$$

This equation yields almost identical results to Eq. 18 in the range $\phi < 0.6$. Since the range of interest in our systems of cohesive particles is $\phi \in\sim [0.2, 0.5]$ we conclude that the use of Eq. 18 is reasonably justified.

The Rumpf equation relates the bulk stresses to the averaged forces over many contacts in the powder bed. The estimated average forces from bulk stresses are, therefore, free of the usually large noise in the forces directly measured between two individual particles[5] (see Figure 1), which is due to the strong dependence on the local properties of the surfaces at contact. Parameters, such as the Young modulus, hardness, asperity profile, and so on, show usually high fluctuations across the particle surface.[48] These fluctuations are probably magnified for particles whose surface is randomly coated with flow additive as in our experimental powders. Thus, the bulk testing method ensures a statistically more meaningful result than would be obtained from single particle contact experiments.

Experimental Results

Effect of surface area coverage of silica additive

The effect of surface roughness and in particular silica coating on the interparticle adhesion force is well known from atomic force microscopy measurements.[16] However, the common situation in powder flow is that particles are compressed by external stresses. A main role of silica additive is then to increase the contact hardness since silica is much harder than polymer ($H \simeq 8.8$ GPa, and $E \simeq 70$ GPa for silica,[48] while $H \simeq 0.3$ GPa, and $E \simeq 6$ GPa for polymer[5]).

Figure 4a displays the estimated F_t as a function of the square root of the estimated interparticle compressive force F_c for xerographic toners with a constant $SAC = 32\%$, but with different particle size. These forces have been obtained from the averaging Rumpf equation (Eq. 14), and using the experimental data on σ_t (for estimating F_t), σ_c (for estimating F_c),

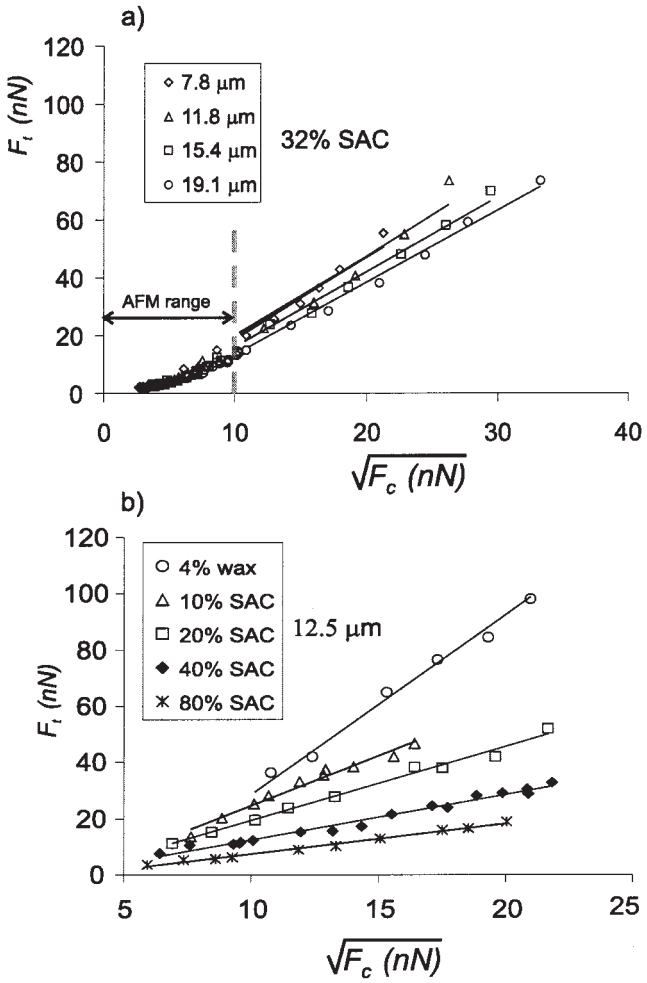

Figure 4. Interparticle adhesion force F_t as a function of the square root of the interparticle compressive force F_c. (a) Toners with the same surface silica additive coverage (32%), but with different particle size. (b) Toners with the same particle size (12.5 μm), but with different surface silica additive coverage.

Data from experiments on a toner with wax additive are also shown. The straight lines are the best linear fits to the data.

and ϕ. Taking into account the accuracy of the bulk measurements, the estimated values of these forces have an accuracy of the order of 1 nN. It is seen that F_t may be well fitted by the equation $F_t = \gamma\sqrt{F_c}$, where γ is approximately the same for all the toners independently of particle size, in agreement with the predicted law for fully plastic behavior (Eq. 5).

Also, in qualitative agreement with Eq. 5, Figure 4b shows that the slope γ decreases as the silica coverage is increased since the addition of silica increases the hardness H of the contact. Because Eq. 5 is valid under the assumption of small-scale-yielding, we will assume that in our case the deformation of the asperities is small as compared to the contact area to meet this condition. Otherwise, our measurements would not be reproducible since the asperities would be irreversibly flattened. The value of γ for the tested powders with the lowest additive coverage (SAC $<\sim$ 10%) is $\gamma \simeq 4 \pm 0.5$ (nN)$^{1/2}$ in good accordance with the theoretical slope calculated from Eq. 5 for polymer-polymer contacts ($\gamma \simeq 3.6$ (nN)$^{1/2}$) using $w \simeq 0.07$ J/m^2, $\nu \simeq 1/3$, $E \simeq 6$ GPa, $H \simeq 0.3$ GPa as typical values. As with respect to the slope for high silica coverage, it is difficult to compare the experimental data with a theoretical prediction. Storakers et al.[17] and Mesarovic and Fleck[27] have studied the mutual indentation of two spheres of unequal material properties through similarity analysis. Yet our problem is even more complicated than that, since at high silica coverage we have predominantly contacts between hard silica nanospheres which are resting on the soft polymer substrate. For this complex contacts a derivation of the maximum pull off force as a function of the compressive force from theoretical grounds is beyond the scope of our work, which is mainly focused on experiments. Nevertheless, our results are in qualitative agreement with the expectation that the increase of the effective contact hardness produces an increase of the slope of F_t vs. $\sqrt{F_c}$. We hope that these results could help in the future to theoretical experts on contact mechanics.

Effect of wax additive

Apart from silica to improve flow properties, some industrial applications demand the use of additional additives such as pigments to provide coloration, specific polymers to fix the pigment to the paper, magnetite additive to facilitate toner handling, special chemicals to control charge levels, and waxes to facilitate the fixing process. Even though each of these components has a unique function, their presence may affect simultaneously other properties, such as interparticle forces. Wax for instance is a very soft material that could enhance adhesion, as shown by Figure 4b, and, thus, worsen flowability. We see in Figure 4b that the addition of wax increases γ as we should have expected from Eq. 7. Moreover, the effect of silica is rapidly lost in the case of waxy toners, suggesting that the silica nanoparticles become embedded in the toner particles.

Effect of size of silica nanoparticles additive and gel content

In Figure 5 we represent the estimated interparticle adhesion force as a function of the interparticle compressive force for the xerographic toners blended with silica nanoparticles of different sizes (8 nm and 40 nm). It is systematically seen that the size of silica nanoparticles has a relevant effect on the force between toner particles with surface additive coverage $100\% > SAC_{ss}$, that is, sufficiently large to ensure that most interparticle contacts are between silica nanoparticles. In those toners we observe that the adhesion force increases with the size of the additive for small compressive forces ($F_c <\sim 100$ nN), whereas for large compressive forces the additive size does not play a major role, in qualitative agreement with Eq. 7. On the other hand, if the surface additive coverage is small (20% *SAC*), contacts between silica nanoparticles are unlikely and accordingly we see that their size has no marked effect on the interparticles forces. We observe, however, that the slope of the plot F_t vs. $\sqrt{F_c}$ (Figure 6) is smaller for the 40 nm silica nanoparticles since for these large sized nanoparticles the real silica coverage ($SAC^* \simeq 13\%$, Eq. 10) is higher than for the smaller nanoparticles ($SAC^* \simeq 4\%$). The experimental data on the toner with 45% gel is compared in Figure 5 with the theoretical curve according to the modified Maugis-Pollock

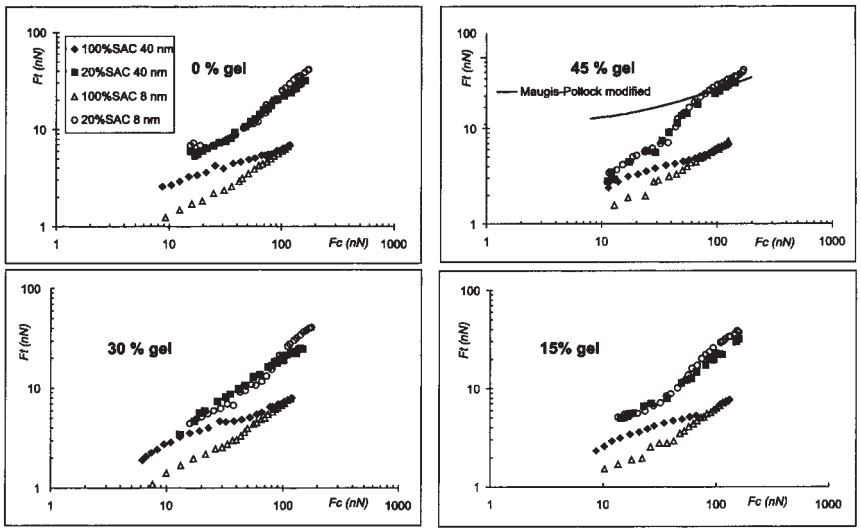

Figure 5. Interparticle adhesion force F_t as a function of the interparticle compressive force F_c for toners with 100% and 20% of surface coverage of silica nanoparticles.

The size of the silica nanoparticles is 8 nm in some toners and 40 nm in others. Each graph corresponds to a different amount of cross linking agent (gel) added to the parent polymer of the toner. The line shown for 45% gel toner corresponds to the theoretical prediction from the modified Maugis-Pollock equation (Eq. 7) assuming a contact between polymer surfaces ($E = 6$ GPa, $\nu = 1/3$, $H = 450$ MPa, $w = 0.07$ J/m^2, $d_{as} = 0.2$ μm).

equation (Eq. 7) calculated assuming a contact between bare polymer asperities. It is seen that at large compressive forces ($F_c >\sim 100$ nN) the theoretical curve fits well to the experimental data on the estimated forces for the toners with low *SAC*. On the contrary, the estimated forces are clearly below the theoretical prediction in the regime of low compressive forces. Let us postpone the discussion on this apparent disagreement.

As for the presence of gel and since it only produces a modest increment of the contact hardness we see that the effect on the adhesion force is not significant as compared to the effect of silica (see Figure 7). Furthermore, the gel also produces a slight increase of the Young modulus (for 30% gel it is measured $E = 5.9$ GPa while for 40% gel $E = 6$ GPa[32]), thus, counteracting the effect of the increase of hardness according to Eq. 7.

Caking of powders

Fine powders usually cake, whether in the storage bin, application equipment, or recovery systems. This tendency is particularly important in cases where beds of powder are allowed to rest for several days or even weeks between periods of use. The caking of powders is basically due to the increase of cohesiveness with time of storage as a consequence of the viscoplastic behavior of interparticle contacts. Our experimen-

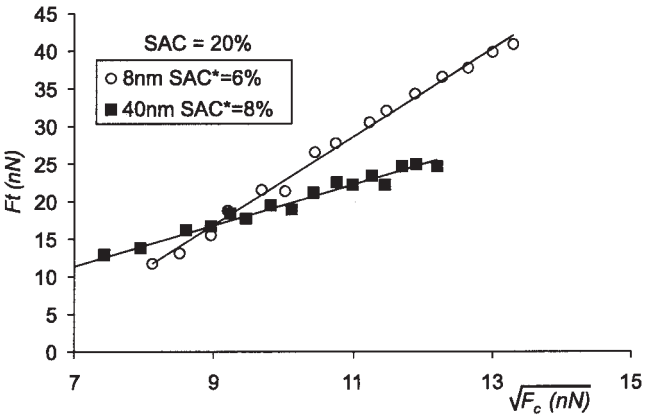

Figure 6. Interparticle adhesion force F_t as a function of the square root of the interparticle compressive force F_c for toners with 20% *SAC*, and 8 nm and 40 nm silica nanoparticles additive, respectively.

The real surface coverage of additive due to aggregation of silica nanoparticles (*SAC**) is indicated in each case. The straight lines are the best linear fits to the data.

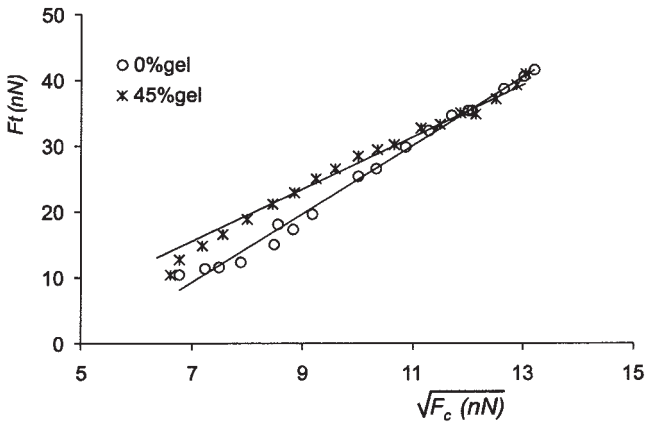

Figure 7. Interparticle adhesion force F_t as a function of the square root of the interparticle compressive force F_c for toners with 0% and 45% of crosslinking agent (gel).

The straight lines are the best linear fits to the data.

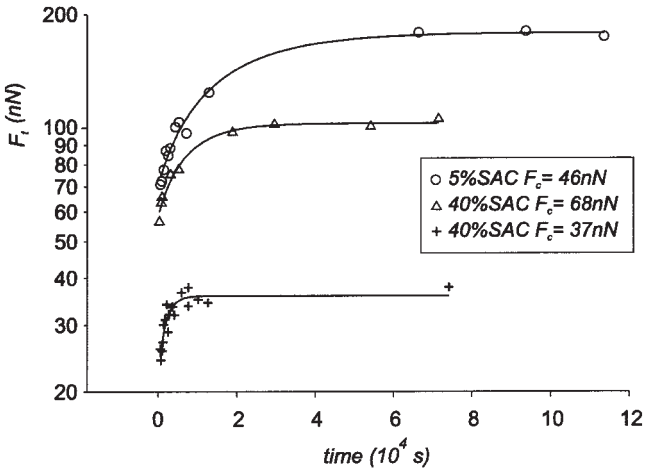

Figure 8. Interparticle adhesion force F_t as a function of the time during which the powder is previously consolidated by an external compressive stress.

The measurements correspond to powders (12.5 μm particle size) with different surface additive coverage and subjected to different consolidation stresses (the estimated interparticle compressive forces are indicated in the inset). The lines are the fits of the function $F_t = y_0 + a(1 - \exp(-t/\tau))$.

tal setup allows to measure the interparticle adhesion force as a function of time of application of the external compressive force. Figure 8 shows some relevant results. Our measurements indicate that the adhesion force rises exponentially to a maximum in a typical time scale τ that depends on the compressive force imposed and on the surface additive coverage. As a general rule τ increases with the level of compressive force previously applied and, for a fixed compressive force, τ decreases as the surface coverage of silica is increased. Thus, the addition of silica to powder prevents hard caking not only by decreasing adhesion, but also by minimizing the viscous component in the behavior of the plastic contacts. To avoid this further complication the experimental data presented in other sections of this article were taken from measurements made within a short time scale ($t <\sim 5$ min $\ll \tau$).

Correlation with measured forces with the atomic force microscope

Figure 9 displays the estimated forces F_t vs. F_c along with the results of F_t^{AFM} vs. F_c^{AFM} (average forces directly measured between two toner particles with the atomic force microscope AFM) at small compressive forces.[5] The data corresponds to two toners of same particle size (12.5 μm) but different surface additive coverage (80% and 10% respectively). Although there is a good correlation between estimated and direct measurements, Eq. 14 underestimates the interparticle adhesion force for a given compressive force, at least in the range of low consolidations that corresponds to the AFM measurements. In spite of the fact that the Rumpf equation is valid only in the case of a homogeneous and isotropic distribution of contacts in a monodisperse assembly of hard spheres, we have concluded elsewhere that the anisotropy in the distribution of contacts and the typical polydispersity of real granular systems play no major role in the averaging of forces.[5] Other phenomena, such as aggregation and/or force chaining need to be evaluated.

Estimation of Contact Forces from Bulk Measurements

Effect of particle aggregation

Figure 10 shows the average interparticle contact forces directly measured with the atomic force microscope,[5] and the contact forces estimated from the Rumpf equation (Eq. 14). The data corresponds to a xerographic toner (12.7 μm particle size) with very low concentration of additive (10% *SAC*, d_s = 8 nm). Given the small coverage of additive we can say that particles contact each other mostly between their bare polymer surfaces, allowing us to plot the modified Maugis-Pollock theoretical prediction (Eq. 7) using the mechanical properties of the bulk polymer. It is seen that within the experimental scatter the AFM experimental data fit well to the modified Maugis-Pollock theoretical curve. On the other hand, the adhesion forces estimated from Eq. 14, based on a homogeneous sharing of the external stress among all interparticle contacts, are clearly below the theoretically predicted and AFM data in the range of consolidations $\sigma_c <\sim 300$ Pa. Yet for $\sigma_c >\sim 300$ Pa the estimated forces from Eq. 14 fit pretty well to the theoretical law (see Figure 10).

In order to better understand the distribution of forces within fine powders we must recall that primary particles are usually aggregated in the fluidized bed due to the strong interparticle attractive forces as compared to particle drag.[49] Aggregates in our cohesive powders are characterized by the number of particles aggregated N, and by the ratio of aggregate radius to particle radius $\kappa = R/a$. We have derived N and κ by fitting experimental data on the sedimentation velocity v_s of the fluidized bed, measured just after turning off the gas supply, to

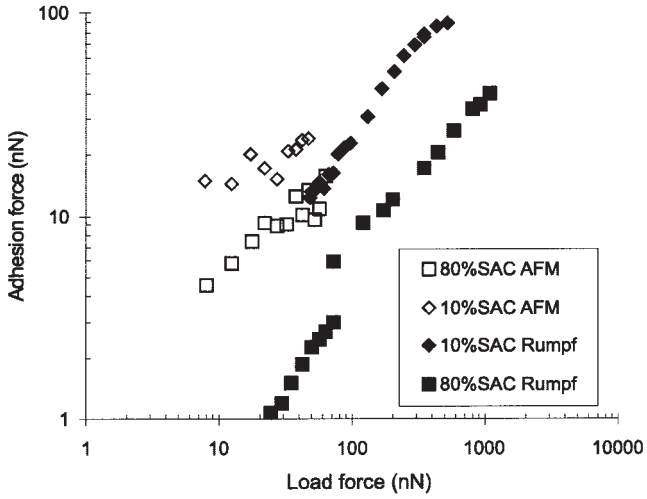

Figure 9. Interparticle adhesion force F_t vs. the interparticle compressive force F_c.

We compare forces directly measured with the AFM (void symbols) with forces estimated from bulk measurements of the tensile yield stress σ_t, and average particle volume fraction ϕ as a function of the consolidation stress σ_c (solid symbols). The two powders tested have the same particle size (12.7 μm) with 80%, and 10% of surface additive coverage, respectively. Contact forces are estimated from the Rumpf equation (Eq. 14).

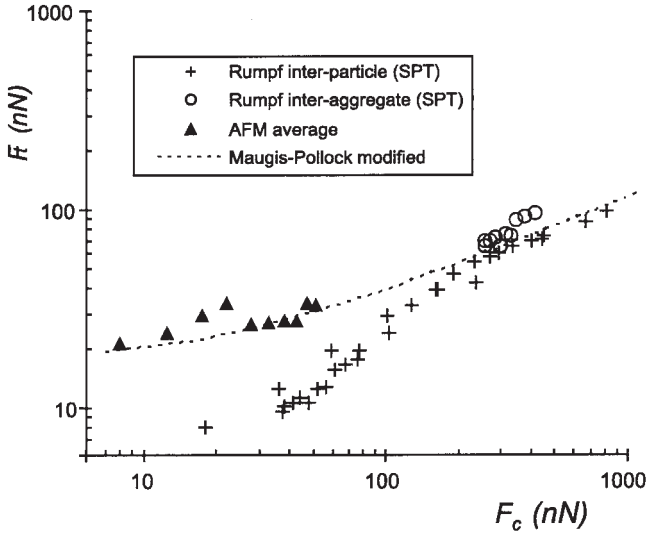

Figure 10. Interparticle adhesion force F_t vs. the interparticle compressive force F_c.

We compare forces directly measured with the AFM, forces theoretically predicted by the modified Maugis-Pollock equation (Eq. 7, $w \simeq 0.07$ J/m^2, $\nu \simeq 1/3$, $E \simeq 6$ GPa, and $H \simeq 0.3$ GPa), forces estimated by means of the Rumpf equation (Eq. 14) from bulk data of the tensile strength σ_t, and particle volume fraction ϕ as a function of the consolidation stress σ_c, and forces estimated by means of the modified Rumpf equation (for $\sigma_c < 100$ Pa). The powder tested has 10% of surface additive coverage and 12.7 μm particle size.

the modified Richardson-Zaki law (see [4] for further explanation)

$$\frac{\nu_s}{\nu_{p0}} = \frac{N}{\kappa}\left(1 - \frac{\kappa^3}{N}\phi\right)^n \tag{20}$$

where ν_{p0} is the settling velocity of an individual particle in the Stokes regime, and $n \simeq 5.6$ for small particle Reynolds number. Recently, Nam et al. have successfully used our technique to characterize aggregates of silica nanoparticles.[50] We show in Figure 11 the expansion curve (particle volume fraction vs. imposed gas velocity) for a fluidized bed of the toner analyzed in this section. We must note that, for this highly cohesive powder, the behavior near the fluid-to-solid transition is rather heterogeneous. As the gas velocity is decreased and the solidlike regime is approached, the strong interparticle forces lead to the formation of transient solidlike regions[52] that favor the development of channels through which the gas escapes rather than being uniformly distributed in the bed. The large heterogeneities in the gas distribution hampers a reliable measurement of the settling velocity near the solidlike regime and rests robustness to the parameters N and k derived exclusively by fitting Eq. 20 to the experimental data. Additional information may be derived form the fluid-to-solid transition. When aggregates jam, we have $k^3/N = \phi_J^*/\phi_J$, being ϕ_J^* the volume fraction filled by the aggregates at jamming. Thus, the modified R–Z equation can be rewritten as

$$\frac{\nu_s}{\nu_{p0}} = \frac{\phi_J}{\phi_J^*}\kappa^2\left(1 - \frac{\phi_J^*}{\phi_J}\phi\right)^n \tag{21}$$

with only one free parameter to be fitted to the experimental data on settling. For this cohesive powder, the jamming transition is precisely recognized on the behavior of ϕ as the gas velocity ν_g is decreased in a fluidization experiment.[8] As the gas velocity is decreased below the jamming threshold, the development of enduring contacts hampers the increase of ϕ as seen in the fluidization curve (see Figure 11). From Figure 11, we infer that the powder jams at $\phi_J \simeq 0.21$. In the case of this highly cohesive powder the volume fraction filled by the aggregates at the jamming transition is $\phi_J^* \simeq 0.5$,[9] thus we obtain $\phi_J/\phi_J^* \simeq 0.21/0.5$. In Figure 12 we have plotted the experimental data on the settling velocity of the fluidized bed, measured just after turning off the gas supply. As expected, there is a rather large scatter of the data for particle volume fractions $\phi >\simeq 0.17$ (compare with the smooth data shown in the inset obtained for the same toner but with 80% SAC). Note, however, that the modified Richardson-Zaki law (Eq. 21) fits reasonably well to the experimental data in the homogeneous fluidization regime. The best fit parameter is $k \simeq 6.12$, that gives $N \simeq 96.5$ and $D = \ln N/\ln k \simeq 2.52$, which is close to the theoretical value for diffusion limited aggregation ($D = 2.5$). For $\phi > 0.17$, the cloud of data points is mostly above the phenomenological law, which might be due to the presence of transient agglomerates of aggregates that accelerate the settling process as compared to the case of a perfectly homogeneous fluidized state.

At the fluid-to-solid transition aggregates are jammed in a random loose packing configuration, and in a range of small pressures rearrange by rolling without breaking internally.[8] These aggregates must disrupt necessarily for consolidation stresses such that the volume fraction filled by the aggregates $\phi^* = \phi\kappa^3/N > 0.64$ (random close packing limit of uniform spheres). According to our experimental data, $\phi^* \simeq 0.64$ for $\phi \simeq 0.27$, which is reached at a consolidation stress $\sigma_c \sim 100$ Pa (Figure 11 (inset)). In fact, we have estimated for other less cohesive toners that the disruption of aggregates initiates at

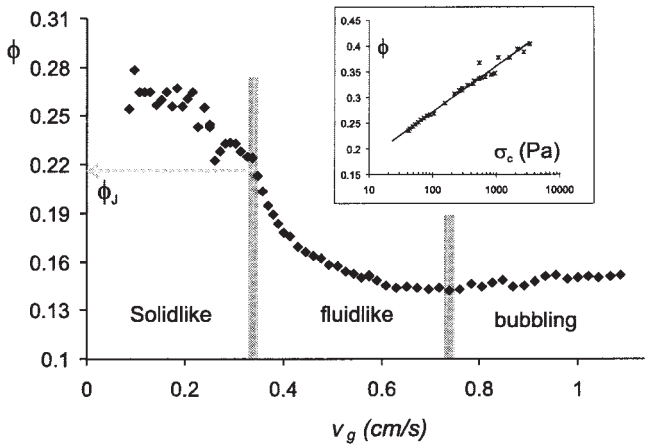

Figure 11. Particle volume fraction ϕ as a function of the fluidizing gas velocity, ν_g for 10% surface additive coverage and 12.7 μm particle size toner.

The vertical line indicates the limits of the different fluidization regimes. Inset: particle volume fraction in the solidlike regime as a function of the consolidation stress. The continuous line is a logarithmic fit to the data.

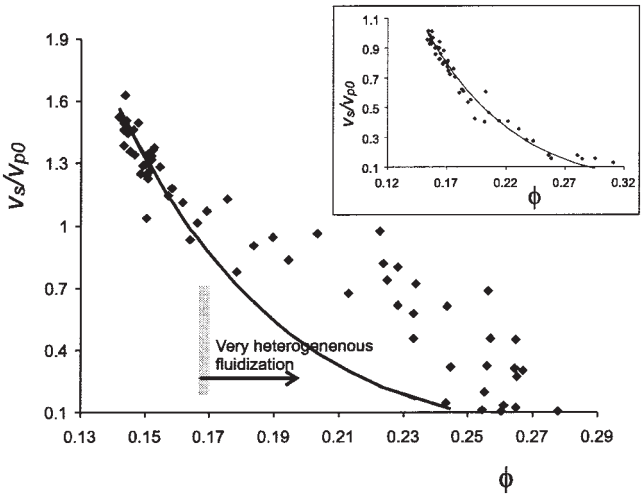

Figure 12. Settling velocity of the top free surface of the fluidized bed measured just after turning off the gas supply as a function of the initial particle volume fraction.

The main graph shows data for 10% surface additive coverage and 12.7 μm particle size toner. The inset shows data for 80% surface additive coverage and 12.7 μm particle size toner. The curves represent the modified Richardson-Zaki law (Eq. 20) fit to the data.

appreciably smaller packing fractions ($\phi^* \simeq 0.53$[9]). Therefore, it is conceivable that in the range $\sigma_c >\sim 300$ Pa aggregates are fully disrupted and the external stress is distributed homogeneously, if force chaining is neglected, among interparticle contacts according to Rumpf's main hypothesis to formulate Eq. 14.

Why does the Rumpf estimation of forces underestimate the adhesion force at very low stresses? A possible answer to this question is that in the system of partially disrupted aggregates the stress is preferentially transmitted through the interaggregate contacts, and, therefore, some of the interparticle contacts within the aggregate act as mere passive spectators. Let us assume that the hierarchy of the structure determined by the aggregate size persists at least in a region of very low stresses that is, aggregate disruption is minimal. Then we must modify Eq. 14 and consider aggregate units as our effective particles. A straightforward choice is to replace the primary particle size (d_p), the interparticle coordination number (ζ), and the particle volume fraction (ϕ) by the aggregate size ($d^* = \kappa d_p$), the effective volume fraction filled by the aggregates ($\phi^* = \phi\kappa^3/N$), and the interaggregate coordination number ($\zeta^* \simeq \pi/2(1-\phi^*)^{-3/2}$), respectively

$$F^* \sim \sigma \frac{\pi d^{*2}}{\zeta^* \phi^*} = \sigma \frac{N}{\kappa} \frac{2d_p^2}{\left(1 - \frac{\kappa^3}{N}\phi\right)^{-3/2} \phi} \tag{22}$$

In Figure 10 we have plotted the estimated forces from Eq. 22 for $\sigma_c < 100$ Pa ($\phi^* < 0.64$), for which aggregate disruption can be expected to be incomplete. It is seen that the estimated contact forces are close to the theoretical curve (especially for $\sigma_c < 70$ Pa). At larger consolidations, the disruption of aggregates is considerable, and it is difficult to find an "effective" particle size. It could be thought that the fraction of "active" contacts η that feel the external stress rises continuously from that corresponding to the aggregate network at small consolidations to $\eta \sim 1$ at $\sigma_c >\sim 300$ Pa. This physical mechanism is formally similar to the force chaining phenomenon observed in systems of hard spheres,[53] where the external stress is carried in effect only by a fraction of "active" contacts. The estimated adhesion force and the estimated compressive force would be then $F_t \sim F_t/\eta$ and $F_c \sim F_c/\eta$, respectively, where F_t and F_c are the estimated forces by the Rumpf equation (Eq. 14). If we now force F_t and F_c to fit the theoretical prediction $F_t \simeq \gamma\sqrt{F_c}$, we can calculate the fraction of active contacts from the equation

$$\eta = \frac{F_t^2}{F_c \gamma^2} \tag{23}$$

Results for η as a function of the consolidation stress σ_c are displayed in Figure 13, where the gray-shaded area reflects the indeterminacy in γ ($\gamma \simeq 4 \pm 0.5$ (nN$^{1/2}$)). There are two plateau regions where respective dynamics is possibly controlled by aggregates and individual particles respectively. In the intermediate region η shows a continuous increase.

The value of η in the small consolidations region can be rationalized from a simple model. Let us assume that in this region aggregates are almost undisrupted. Within the ramified aggregates, the points of interaggregate contacts must be connected mostly through chains of particles that transmit the external stress across the aggregate while the rest of particles within the aggregate do not play an active role (see Figure 13 inset). The interaggregate coordination number in their loosely packed state is $\zeta^* \simeq 5$, which must be the order of active chains inside the aggregate. Taking into account that, for the powder tested, there is an average of $N \simeq 100$ particles per aggregate

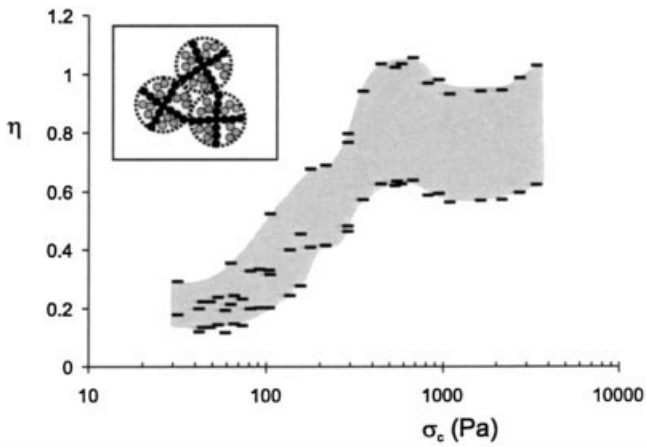

Figure 13. Fraction of active contacts $\eta = F_t^2/(\gamma^2 F_c)$ as a function of the consolidation stress σ_c (toner with 12.5 μm particle size and 10% *SAC*).

The gray-shaded area represents the standard deviation of the measurements due to the indeterminacy in γ ($\gamma \simeq 4 \pm 0.5$ (nN)$^{1/2}$). The inset is a two-dimensional (2-D) representation to illustrate the force chaining mechanism in the transmission of the external stress, when particles are distributed in aggregates (black particles would carry in effect most of the stress whereas the gray particles act just as passive spectators).

and that the average ratio of the aggregate size to particle size is $k \simeq 6$, we would have $N_{act} \sim k\zeta^* \sim 30$ particles belonging to the active network within the aggregate. This rough estimation gives a fraction of active contacts $N_{act}/N \sim 0.3$, which agrees with the result shown in Figure 13 at low consolidations. Thus, a simplified physical picture of the granular skeleton at very low stresses might consist of force chains with a correlation length of the order of the aggregate size carrying in effect the external stress. As the aggregates are disrupted, more and more particles join to the active network, and η increases up to reach a value close to one for a sufficiently high stress. At this level of stress most of the particles would carry the external stress. It could be argued that some force chains could persist even though aggregates are fully disrupted, but polymer particles are not hard, and simulations[54] and experiments[55] indicate a homogeneous sharing of stress in soft particle granular systems. Within the accuracy of our analysis (Figure 13), we can say that at least 60% of contacts are active for $\sigma_c > \sim 300$ Pa.

It must be remarked that even though particle aggregation affects the transmission of external stresses, thus, invalidating the original Rumpf equation, it does not affect qualitatively our result relative to the effect of the size of silica nanoparticles on the interparticle adhesion force at low compressive forces (Figure 6). Since, for 100% SAC, the size of toner particle aggregates is similar for 8 nm and for 40 nm silica nanoparticles[9] the effect of considering the modified Rumpf equation (Eq. 22) would be the same in both cases.

Conclusions

Interparticle contact forces have been estimated from experimental measurements of bulk stresses and packing fraction of fine powders. As a general rule, the interparticle adhesion force increases proportionally to the square root of the interparticle compressive force ($F_t \simeq \gamma\sqrt{F_c}$), suggesting that interparticle contacts undergo plastic deformation even at very small compressive forces. In qualitative agreement with the theory for plastic contacts, we have observed that the slope γ depends critically on the contact hardness H, which can be modified by means of surface additives, such as the silica nanoparticles used in xerography to improve powder flow. As the level of coating of these hard nanoparticles is increased, the slope γ decreases as plasticity theory predicts. Another effect of coating with silica nanoparticles is to control the typical radius of curvature of the surfaces at contact, which is important to the adhesion force in the regime of small compressive forces. In agreement with the theory we have seen that the increase of the size of a silica nanoparticles produces an increase of the adhesion force at small compressive forces (comparable to the attractive force $F_{at} = \pi w d_{as}^* \sim 20$ nN), whereas this effect is not marked at large compressive forces. On the other hand, the slope γ increases with the presence of wax additive, used in xerography to facilitate the fixing process, since this material is quite soft. The moderate increase of contact hardness by use of cross-linking agent produces a slight decrease of the slope γ as predicted by theory. In close relation with the common tendency of fine powders to cake, our measurements of the adhesion force as a function of the time of application of the compressive force reveal a viscous behavior of the contact characterized by a typical time scale that is a function of the surface properties and the compressive force externally imposed. Finally, our estimated forces from bulk measurements are correlated to interparticle forces directly measured with the AFM. We suggest, however, that, especially at small compressive forces, the aggregation of fine particles should be considered as an important phenomenon for the distribution of external stresses within the bulk of the powder. The distribution of stresses among particle aggregates would give rise to a physical picture consisting of force chains transmitting most of the compressive stress with a correlation length of the order of the aggregate size that shortens as the magnitude of the compressive stress is increased and, thus, aggregates are progressively disrupted. Even though our experimental study is obviously restricted to a special class of cohesive powders, it highlights a central problem to a scientific understanding of cohesive powders behavior, namely the nonlinearity in contact forces and particle aggregation. For instance, in a recent article[9] it has been shown that the compaction of cohesive particles can be understood from the configurational structure of the jammed clusters at the fluid-to-solid transition. Snow avalanches are another example where the aggregation of cohesive particles must have important implications as indicated by recent experiments on avalanches of artificially made clusters of beads.[11] Therefore, a proper modeling of contact forces and the consideration of particle aggregation must be concerns, mostly obviated so far, in the formulation of numerical simulations dealing with the behavior of real cohesive powders.

Acknowledgments

This research has been supported by Xerox Foundation, Xerox Corporation, and Spanish Government Agency Ministerio de Ciencia y Tecnologia (contract BFM2003-01739).

Literature Cited

1. Yang RY, Zou RP, Yu AB. Computer simulation of the packing of fine particles. *Phys Rev E.* 2000;62:3900–3908.
2. Nase ST, Vargas WL, Abatan AA, McCarthy JJ. Discrete characterization tools for cohesive granular material. *Powder Technol.* 2001; 116:214–223.
3. Forsyth AJ, Hutton SR, Osborne CF, Rhodes MJ. Effects of interparticle force on the packing of spherical granular material. *Phys Rev Lett.* 2001;244301(1–4).
4. Castellanos A, Valverde JM, Quintanilla MAS. Aggregation and sedimentation in gas-fluidized beds of cohesive powders. *Phys Rev E.* 2001;041304(1–7).
5. Quintanilla MAS, Castellanos A, Valverde JM. Correlation between bulk stresses and interparticle contact forces in fine powders. *Phys Rev E.* 2001;031301(1–9).
6. Fichman M, Pnueli D. Sufficient conditions for small particles to hold together because of adhesion. *Trans ASME J Appl Mech.* 1985;52: 105–108.
7. Goddard JD. On sticky-sphere assemblies. In: Vermeer PA, Diebels S, Ehlers W, Herrmann HJ, Luding S, Ramm E. *Continuous and Discontinuous Modelling of Cohesive-Frictional Materials.* Berlin: Springer; 2001:143–148.
8. Valverde JM, Quintanilla MAS, Castellanos A. Jamming threshold of dry fine powders. *Phys Rev Lett.* 2004;92:258303 (1–4).
9. Castellanos A, Valverde JM, Quintanilla MAS. Physics of compaction of fine cohesive powders. *Phys Rev Lett.* 2005;94:75501(1–4).
10. Castellanos A. The relationship between attractive interparticle forces and bulk behaviour in dry and uncharged fine powders. *Adv Phys.* 2005;54, 263–376.
11. Olson J, Priester JM, Luo J, Chopra S, Zieve RJ. Packing fractions and maximum angles of stability of granular materials. *Phys Rev E.* 2005; 72:031302(1–6).
12. Gady B, Schleef D, Reifenberger R, Rimai D, DeMejo LP. Identification of electrostatic and van der Waals interaction forces between a

micrometer-size sphere and a flat substrate. *Phys Rev B.* 1996;53: 8065–8070.
13. Hamaker HC. The London-Van der Waals attraction between spherical particles. *Physica.* 1937;1058–1072.
14. Krupp H. Particle adhesion, theory and experiment. *Adv Colloid Interface Sci.* 1967;1:111–239.
15. Rietema K. *The Dynamics of Fine Powders.* London: Elsevier; 1991.
16. Ott ML, Mizes HA. Atomic-force microscopy adhesion measurements of surface-modified toners for xerographic applications. *Colloids and Surfaces A.* 1994;87:245–256. Zhou H, Gotzinger M, Peukert W. The influence of particle charge and roughness on particle–substrate adhesion. *Powder Technol.* 2003;135:82–91.
17. Storakers B, Biwa S, Larson PL. Similarity Analysis of Inelastic Contact. *Int J Solids Struct.* 1997;34:3061–3083.
18. Johnson KL, Kendall K, Roberts AD. Surface energy and contact of elastic solids. *Proc R Soc London Ser A.* 1971;324:301–313.
19. Derjaguin BV, Muller VM, Toporov YP. Effect of contact deformations on adhesion of particles. *J Colloid Interface Sci.* 1975;53:314–326.
20. Barthel E. On the description of the adhesive contact of spheres with arbitrary interaction potentials. *J Colloid Interface Sci.* 1998;200:7–18.
21. Maugis D. Adhesion of spheres—the JKR-DMT transition using a dugdale model. *J Colloid Interface Sci.* 1992;150:243–269.
22. Greenwood JA, Johnson KL. An alternative to the Maugis model of adhesion between elastic spheres. *J Phys D.* 1998;31:3279–3290.
23. Chow TS. Nanoadhesion between rough surfaces. *Phys Rev Lett.* 2001;86:4592–4595.
24. Vu-Quoc L, Zhang X, Lesburg L. Normal and tangential force-displacement relations for frictional elasto-plastic contact of spheres. *Int J Solids Struct.* 2001;38:6455–6489.
25. Maugis D, Pollock HM. Surface forces, deformation and adherence at metal microcontacts. *Acta Metall.* 1984;32:1323–1334.
26. Mesarovic SD, Johnson KL. Adhesive contact of elastic-plastic spheres. *J Mech Phys Solids.* 2000;48:2009–2033.
27. Mesarovic SD, Fleck NA. Frictionless indentation of dissimilar elastic-plastic spheres. *Int J Solids Struct.* 2000;37:7071–7091.
28. Wu CY. University of Aston. Birmingham, 2001. Finite element analysis of particle impact problems. Ph.D. Thesis.
29. Johnson KL. *Contact Mechanics.* Cambridge: Cambridge University Press; 1985.
30. Kogut L, Etsion I. Elastic-plastic contact analysis of a sphere and a rigid flat. *J Appl Mech.* 2002;69:657–662.
31. Quintanilla MAS, Castellanos A, Valverde JM. Interparticle contact forces in fine cohesive powders. Theory and experiments. *Proc Appl Math Mech.* 2003;3:206–207.
32. Ahuja SK. Private communication.
33. Massimilla L, Donsi G. Cohesive forces between particles of fluid-bed catalysts. *Powder Technol.* 1976;15:253–260. Mason TG, Levine AG, Ertas D, Halsey TC. Critical angle of wet sandpiles. *Phys Rev E.* 1999;60:5044–5047.
34. Valverde JM, Ramos A, Castellanos A, Watson PK. The tensile strength of cohesive powders and its relationship to consolidation, free volume and cohesivity. *Powder Tech.* 1998;97:237–245.
35. Valverde JM, Castellanos A, Ramos A, Perez AT, Morgan MA, Watson PK. An automated apparatus for measuring the tensile strength and compressibility of fine cohesive powders. *Rev Sci Instrum.* 2000; 71:2791–2795.
36. Valverde JM, Castellanos A, Quintanilla MAS. The memory of granular materials. *Contemp Phys.* 2003;44:389–399.
37. Carman PC. Fluid flow through granular beds. *Trans Inst Chem Engrs.* 1937;15:150–156.
38. Rumpf H. Grundlagen und Methoden des Granulierens. *Chem Ing Tech.* 1958;30:144–158.
39. Emeriault F, Chang CS. Interparticle forces and displacements in granular materials. *Comput Geotech.* 1997;20:223–244.
40. Radjai F, Wolf DE, Jean M, Moreau JJ. Bimodal character of stress transmission in granular packings. *Phys Rev Lett.* 1998;80:61–64.
41. Storakers B, Fleck NA, McMeeking RM. The visco-plastic compaction of composite powders. *J Mech Phys Solids.* 1999;47:785–815.
42. Martin CL. Elasticity, fracture and yielding of cold compacted metal powders. *J Mech Phys Solids.* 2004;52 (8):1691–1717.
43. Poquillon D, Lemaitre J, Baco-Carles V, Tailhades P, Lacaze J. Cold compaction of iron powders—relations between powder morphology and mechanical properties Part 1: Powder preparation and compaction. *Powder Technol.* 2002;126:65–74.
44. Suzuki M, Makino K, Yamada M, Iinoya K. Study on the coordination number in a system of randomly packed, uniform-sized spherical particles. *Int Chem Eng.* 1981;21:482–488.
45. Nakagaki M, Sunada H. Theoretical studies on structures of the sedimentation bed of spherical particles. *Yakugaku Zashi.* 1968;88:651–655.
46. Jaraiz E, Kimura S, Levenspiel O. Vibrating beds of fine particles. Estimation of interparticle forces from expansion and pressure drop experiments. *Powder Technol.* 1992;72:23–30.
47. Watson PK, Mizes H, Castellanos A, Perez AT. *The Packing of Fine, Cohesive Powders.* In Behringer R, Jenkins JT. Powders & Grains 97; Rotterdam: Balkema, 1997:109–112.
48. See applications notes at http://www.micromaterials.co.uk/
49. Chaouki J, Chavarie C, Klvana D, Pajonk G. Effect of interparticle forces on the hydrodynamic behaviour of fluidized aerogels. *Powder Technol.* 1985;43:117–125.
50. Nam CH, Pfeffer R, Dave RN, Sundaresan S. Aerated vibrofluidization of silica nanoparticles. *AIChE J.* 2004;50:1776–1785.
51. Tatek Y, Stoll S, Ouali L, Pefferkorn E. Structure and cohesion of weakly agglomerated fractal systems. *Powder Technol.* 2004;143: 117–129.
52. Valverde JM, Quintanilla MAS, Castellanos A, Mills P. Experimental study on the dynamics of gas-fluidized beds. *Phys Rev E.* 2003;67: 016303(1–5).
53. Behringer RP, Howell D, Kondic L, Tennakoon S, Veje C. Predictability and granular materials. *Physica D.* 1999;133:1–17. Makse HA, Johnson DL, Schwartz LM. *Phys Rev Lett.* 2000;84:4160–4163.
54. Thornton C, Antony SJ. Quasi-static deformation of particulate media. *Phil Trans R Soc Lond A.* 1998;356:2763–2782.
55. Erikson JM, Mueggenburg NW, Jaeger HM, Nagel SR. Force distributions in three-dimensional compressible granular packs. *Phys Rev E.* 2002;66:040301(1–4).

Manuscript received July 15, 2005, revision received Oct. 18, 2005, and final revision received Dec. 13, 2005.